ULTRASOUND NEWS

July 2025

Original article | Open access
Published: 30 May 2025

Ultrasound-based statistical shape modeling for prognosis in unstable hip dysplasia

E. M. van Bussel, L. van Marle, … R. Sakkers

+ Show authors

The Ultrasound Journal **17**, Article number: 26 (2025)

Ultrasound-based statistical shape modeling for prognosis in unstable hip dysplasia

E. M. van Bussel[1*†], L. van Marle[1†], J. M. Bonsel[2], D. de Vrij[1], H. Weinans[1] and R. Sakkers[1]

Abstract

Background Current methods to classify developmental dysplasia of the hip (DDH) on ultrasound (US) images, such as the Graf method, provide limited prognostic information. This study aimed to improve the prediction of the clinical course and outcome at age five of decentered hips, diagnosed on the first US made in the first months after birth, by identifying acetabular shape variants on these US images using a statistical shape model (SSM).

Patients and Methods US images of the hip were retrieved from a single-center retrospective cohort of patients with DDH Graf type D/III/IV. A SSM was created from the US images made at initial diagnosis.. The association between the identified acetabular shape variants and an unfavorable outcome (residual DDH at age five and open reduction and/or a pelvic osteotomy before age five) was established with multivariable regression models.

Results 92 decentered dysplastic hips with full history could be retrieved from the database and were included. At age five, 12 patients (13%) had undergone open reduction, 13 (14%) had a pelvic osteotomy, and 32 (35%) patients showed residual DDH. Four shape variants represented 95% of the variance in acetabular shape. Mode 4 was associated with an unfavorable outcome (odds ratio (OR): 1.80 (95% CI 1.12–2.90). Mode 1 was associated with less risk on open reductions or pelvic osteotomies (OR: 0.56 (95% CI 0.33–0.96).

Conclusions A potential new method of analyzing US images for DDH using SSM established four distinct acetabular shapes on neonatal US images with unstable DDH, of which two were associated with outcomes at five years of age. This tool could serve as a basis for a better prediction of outcome and a more personalized and effective guide for treatment.

Keywords Ultrasound, Neonatal, DDH, Unstable, Dysplasia, Hip, SSM, Statistical shape modeling, SSM

Results

92 decentered dysplastic hips with full history could be retrieved from the database and were included. At age five, 12 patients (13%) had undergone open reduction, 13 (14%) had a pelvic osteotomy, and 32 (35%) patients showed residual DDH. Four shape variants represented 95% of the variance in acetabular shape. Mode 4 was associated with an unfavorable outcome (odds ratio (OR): 1.80 (95% CI 1.12–2.90). Mode 1 was associated with less risk on open reductions or pelvic osteotomies (OR: 0.56 (95% CI 0.33–0.96).

Conclusions

A potential new method of analyzing US images for DDH using SSM established four distinct acetabular shapes on neonatal US images with unstable DDH, of which two were associated with outcomes at five years of age. This tool could serve as a basis for a better prediction of outcome and a more personalized and effective guide for treatment.

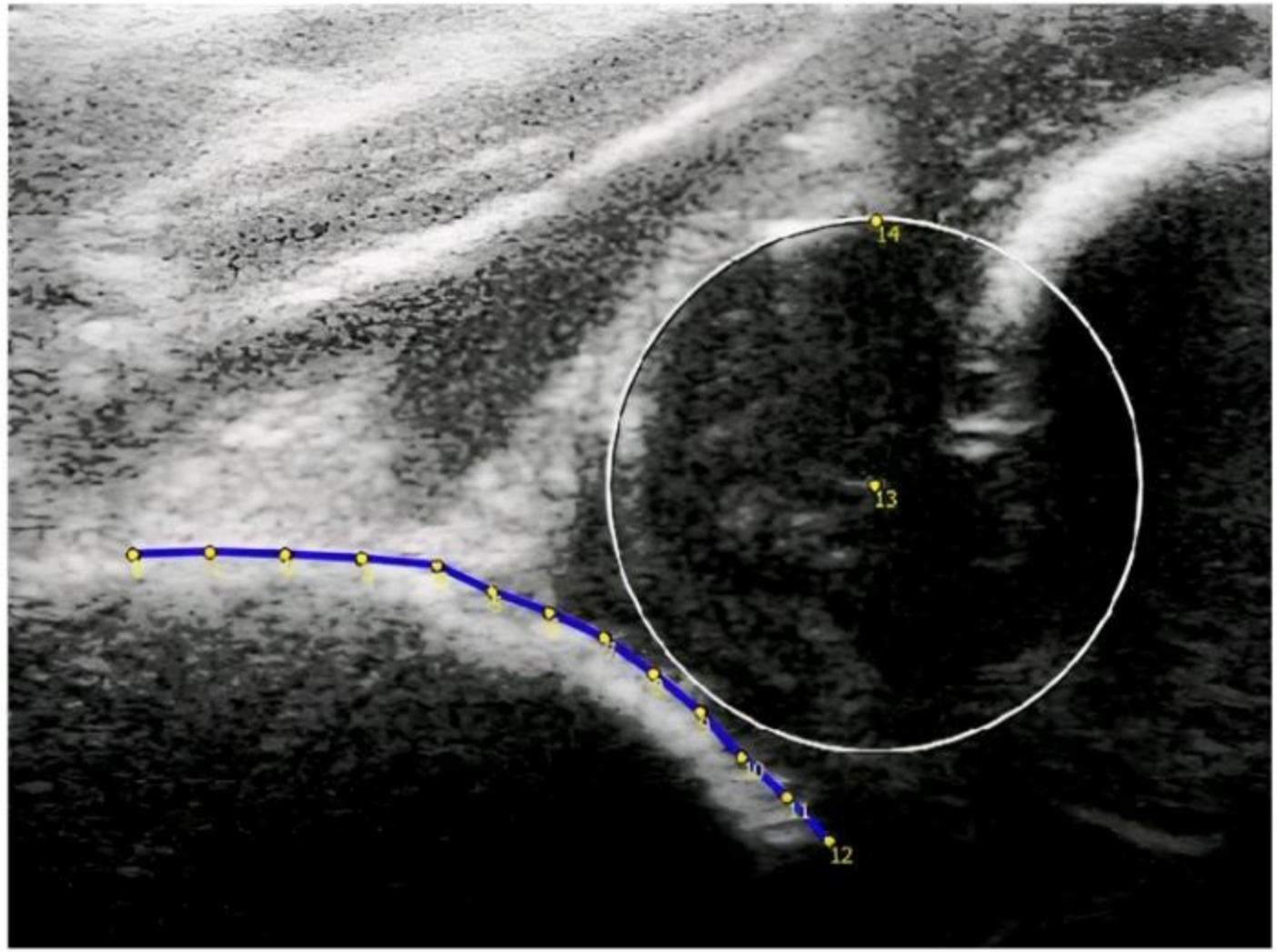

Fig. 1 Baseline ultrasound of a decentered hip with points 0–12 at the bony contour of the ilium and acetabulum. Points 13 and 14 are placed on a best-fitted circle drawn over the femoral head

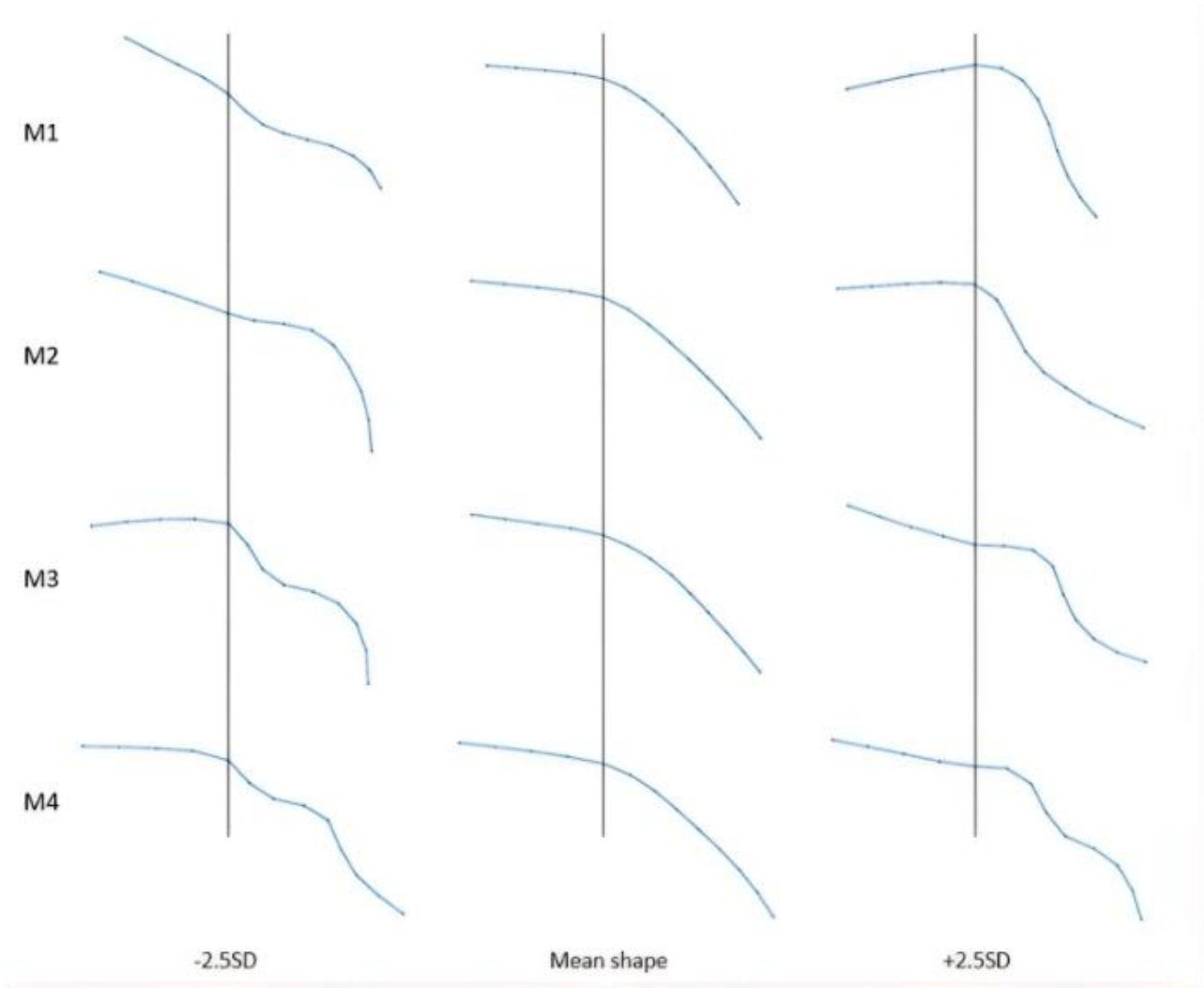

Fig. 4 First four shape modes explaining 95% of shape variation. For clarity purposes, −2.5SD, 0SD, and + 2.5 SD from the mean shape are depicted for each mode. A vertical line is drawn through point 4 in all shapes, representing the start of the slope of the bony acetabular roof

Multiparametric ultrasound imaging of the urinary bladder beyond urine volume measurements. A pictorial essay.

Demosthenes D Cokkinos[1], Vasileios Rafailidis[2], Ioannis Melissovas[3], Avi Beck[4], Abraham Levitin[4], Sasan Partovi[4]

[1]Imaging Department, Lefkos Stavros-The Athens Clinic, Athens, Greece, [2]Department of Radiology, AHEPA University Hospital, Aristotle University of Thessaloniki, Thessaloniki, Greece, [3]Radiology Department, Evangelismos Hospital, Athens, Greece, [4]Section of Interventional Radiology, Imaging Institute, Cleveland, OH, USA

Abstract

Ultrasound of the urinary bladder detects diverse and complex pathology. This manuscript deals with various bladder diseases imaged with multiparametric ultrasound, including contrast enhanced ultrasound.

Keywords: urinary bladder; ultrasound; CEUS

Introduction

The urinary bladder is routinely imaged with ultrasound (US). Some pathologies are diagnosed with standard B-mode US, while others are complex, requiring multiparametric US, including contrast enhanced US (CEUS), computed tomography (CT) or magnetic resonance imaging (MRI).

Indications for bladder US

1. Bladder volume, residual urine volume post micturition

Most devices enable automatic measurements using the standard Poston formula [1]. After micturition, the bladder is re-scanned and residual urine volume is measured. Significantly increased residual urine volume suggests urinary retention.

2. Diverticula

Diverticula are protrusions of bladder urothelium and mucosa via the muscularis propria, due to defects between detrusor muscle fibers. Thus, parts of bladder lumen protrude outwards (fig 1).

Upon chronic obstruction, muscle bladder wall bundles stretch, acquiring a coarse interwoven texture ("trabeculation"). In patients overcoming obstruction during micturition, bladder pressure increases [2], forming small cellules which infiltrate through the wall, forming diverticula.

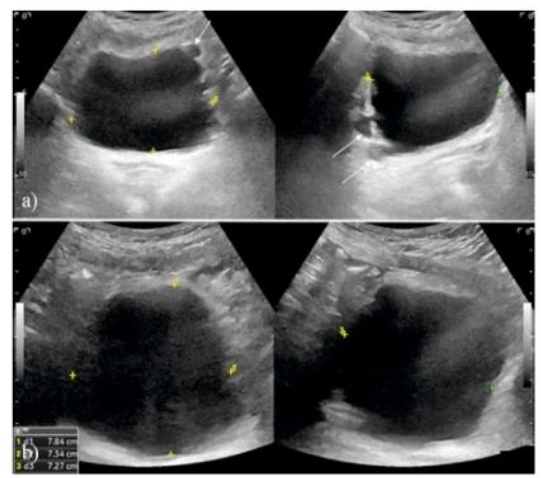

Fig 1. Patient with multiple sclerosis shows trabeculated bladder and diverticula (arrows in a). Bladder volume is pre-voiding 230 mL and post-voiding 220 mL (b), due to urinary retention.

Received 24.11.2024 Accepted 02.01.2025
Med Ultrason
2025, Vol. 27, No 2, 227-233
Corresponding author: Dr Demosthenes D Cokkinos
Imaging Department,
Lefkos Stavros – The Athens Clinic,
5 Dorylaiou. Athens 11521, Greece
Phone: +30 6974 313935
Email: demoscokkinos@gmail.com

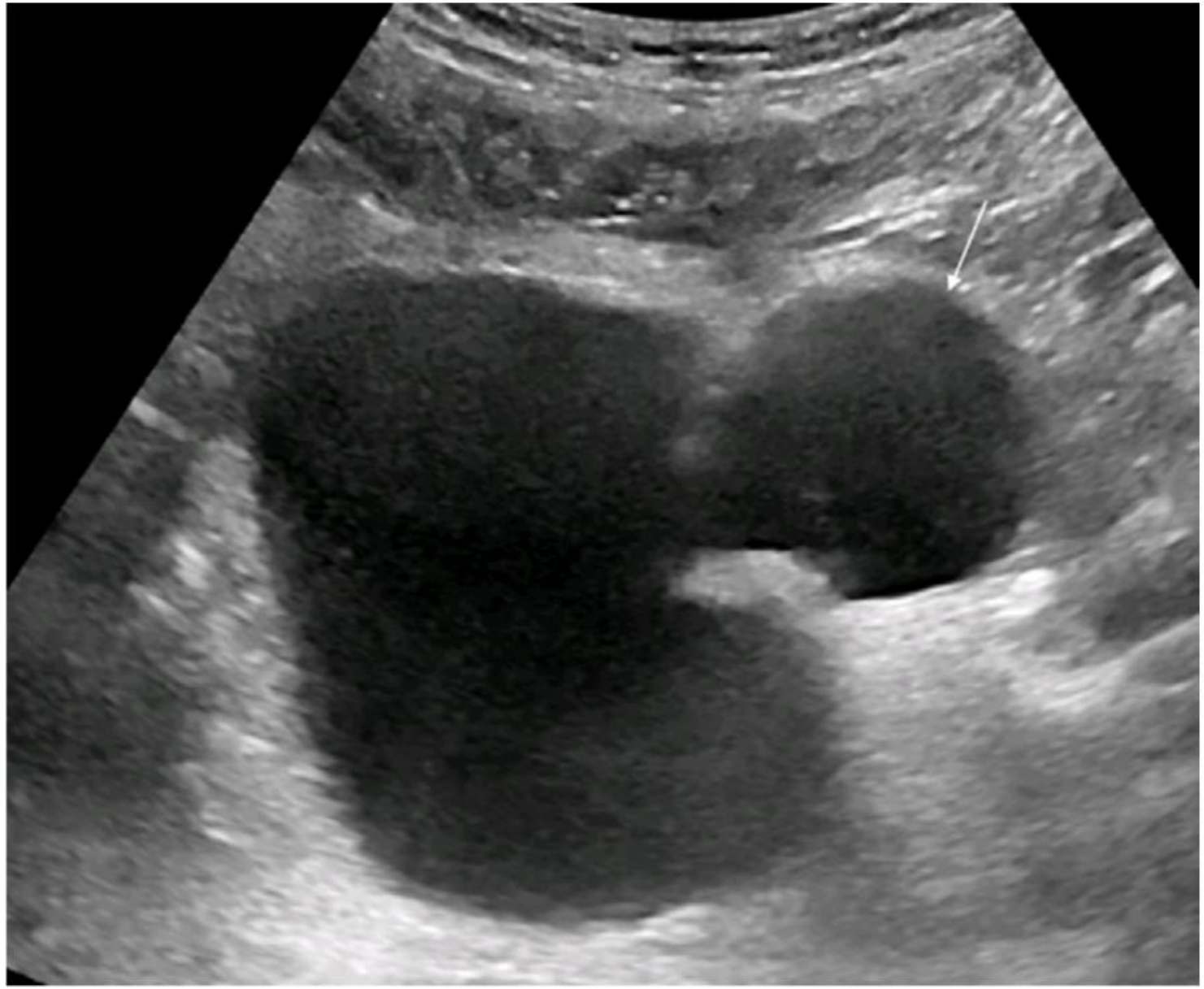

Fig 19. A medical erection-helping device is noted next to the bladder (arrow). History is needed to differentiate this from a diverticulum on US.

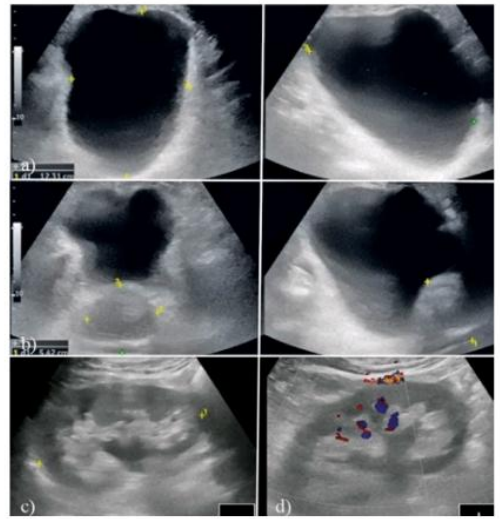

Fig 8. The bladder is distended (a: urine volume almost 700 cc) secondary to prostatic gland enlargement (b: volume of 73 cc), with hydroureteronephrosis of right (c) and left (d) renal collecting systems.

pertrophic and trabeculated secondary to bladder outlet obstruction (fig 8) [5].

6. Debris and blood clots

Debris represents mobile, echogenic particles in urine within the pelvicalyceal system, ureters or bladder [6]. It appears on US as small dependent echogenic particles, mobile when changing patient positions. Large debris quantities may appear layered (fig 9). CEUS differentiates enhancing tumors from adjacent hemorrhagic debris/blood clot or puss (fig 10, fig 11).

7. Fistulae

Fistulae are abnormal communications between two epithelialised surfaces. In the bladder, fistulae form between bladder and vagina/uterine cavity (vesicovaginal fistulae), gastrointestinal tract (fig 12) (colovesical, ileovesical, rectovesical fistulae), urethra, skin and abdominal wall.

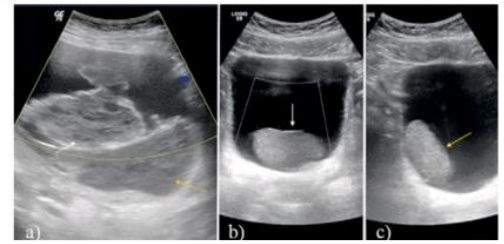

Fig 9. Two different patients with bladder debris. Patient 1: Debris is chronic (a) since two separate layers have formed (white and yellow arrows). Patient 2: Debris has a mass-like configuration (b, c), though it is mobile with altered patient positions (white arrow in supine position, yellow arrow in right decubitus position.

8. Cystitis

Sonographic findings of cystitis include [7] bladder wall hypertrophy (fig 13), mucosal irregularity, debris, periserosal edema, bladder wall calcification. Underlying findings include tumor, foreign body, diverticulum. In emphysematous cystitis, US demonstrates echogenic free air within the bladder wall and wall thickening.

9. Trauma

On CEUS a hematoma adjacent to the bladder appears as a biconvex non-enhancing area (fig 14). CEUS can also be performed instilling diluted contrast agent through the catheter (retrograde transurethral CEUS) (fig 15) [8].

10. Ureterocele

Ureteroceles are congenital saccular dilatations of the distal ureter, herniating inside the bladder lumen due to abnormal ureterovesical junction (UVJ). On US ureteroceles appear as cystic lesions of dilated distal ureter (fig

Fig 10. A motorcycle accident victim undergoes B-mode US shortly after midnight (time reads 00:18 in red box in a). The right kidney is heterogenous with small fluid collection in Morison's pouch (arrow in a). Echogenic material is seen within the bladder (arrow in b). CEUS reveals right kidney laceration (arrow in c). The bladder hemorrhagic content does not enhance (arrows in d). The CEUS examination is completed within 5 minutes by 00:23 (time in red box in d). Right kidney trauma is confirmed on CECT (arrow in e) much later (time in red box in e reads 01:58).

US depicts diverticula as anechoic lesions outside of the bladder lumen. If pedunculated, an isthmus connects the diverticulum to the bladder. A large diverticulum is difficult to differentiate from the lumen (fig 2).

3. Bladder calculi

Bladder stones form within the bladder or migrate from the kidneys. On US stones present as echogenic lesions with posterior shadow [3] (fig 3). Bladder tumors are differentiated from stones by changing the patient's position: stones move, while masses do not.

4. Tumors

On US, bladder tumors appear as echogenic wall-adherent masses, occasionally with calcifications. Tumors may warrant differentiation from debris. When the patient's position changes, masses are immobile, while debris and hemorrhagic material can change position. Color Doppler and techniques such as Microvascular Imaging (MVI) show perfusion in tumors, while debris shows no perfusion (fig 4). CEUS better differentiates blood clot without contrast uptake from enhancing tumor masses [4] (fig 5, fig 6).

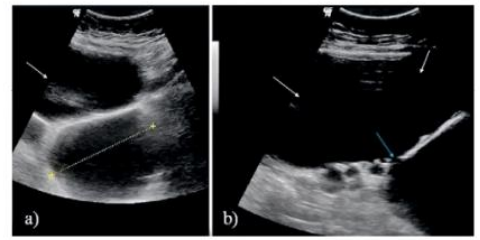

Fig 2. Large bladder diverticula are seen on B-mode US. Due to their size, differentiation from the actual bladder lumen (white arrows in a, b) remains challenging. Communicating points (blue arrow in b) between lumen and diverticula help to differentiate bladder lumen from diverticula.

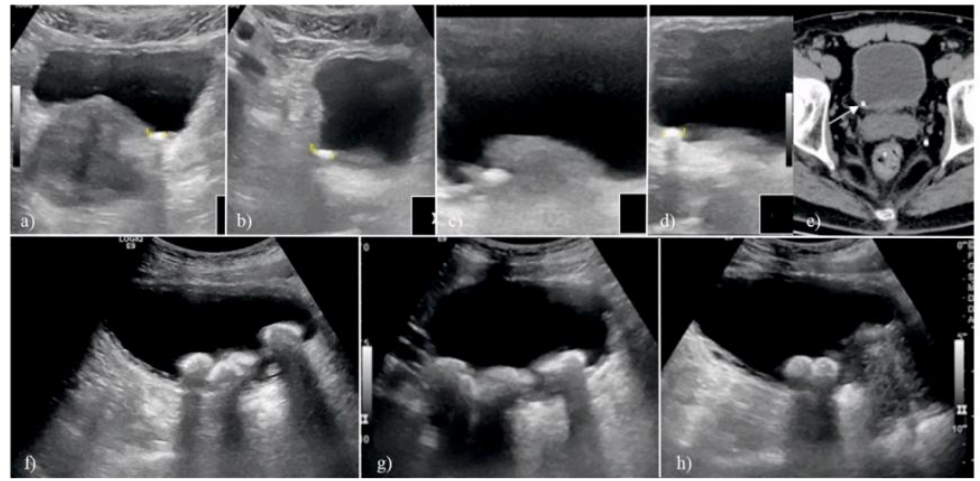

Fig 3. Two patients with bladder stones. Patient 1: Stones in the bladder move with patient position changing: a) supine, b) right decubitus, c) left decubitus, d) supine; e) CT confirms the stones (arrow). Patient 2: Stones in the bladder move while changing patient positioning (f, g, h).

In patients with a post cystectomy due to bladder malignancies, the urine is collected in a surgically created external pouch or in an ileal conduit (fig 7).

5. Benign prostatic hyperplasia (BPH)

BPH is common in elderly men. The prostate is enlarged (volume over 30 mL). Residual urine volume post micturition is increased, and the bladder wall appears hy-

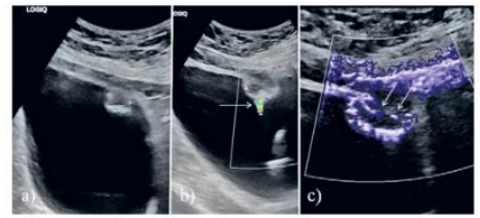

Fig 4. Incidental finding of a bladder TCC. B-mode US (a) shows a papillary projection. Color Doppler (b) shows no perfusion. A twinkling artifact (arrow) is caused by denser lesion parts. MVI technique (c) visualizes internal linear blood flow signals delineating blood vessels (arrows), suggesting a tumor. There are also artifactual signals at the lesion's margin.

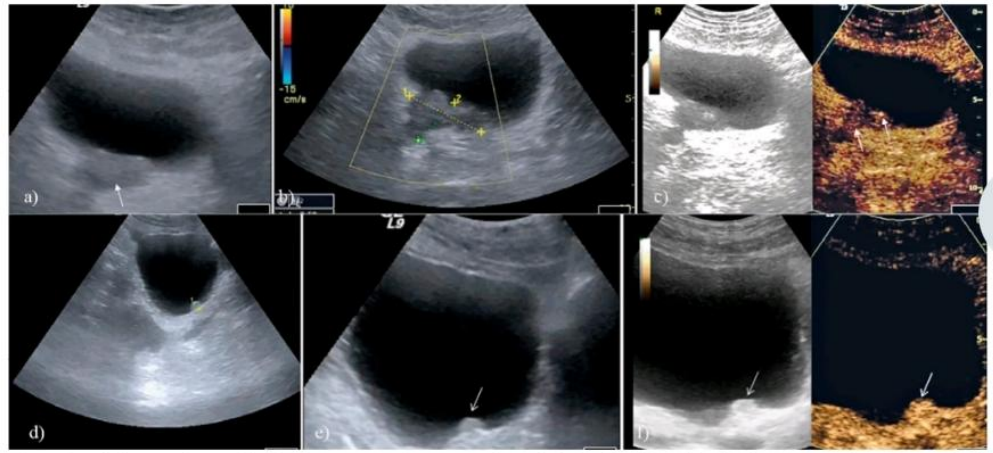

Fig 5. Two different patients with bladder tumors. Patient 1: an echogenic lesion invades a diverticulum on B-mode US (arrow in a), with no perfusion on color Doppler US (between calipers in b). On CEUS the lesion enhances (arrows in c). Patient 2: a 6 mm echogenic lesion is noted on B-mode US (between calipers in d, arrow in e). On CEUS the lesion enhances (arrow in f).

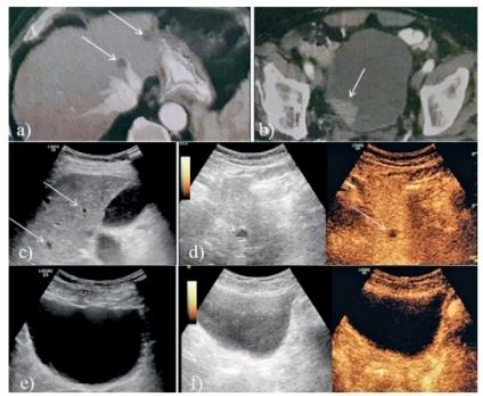

Fig 6. A patient with known bladder neoplasia undergoes CECT (a, b), demonstrating hypoattenuating hepatic cysts (arrows in a). The bladder mass is noted (arrow in b). After 8 months of treatment, the liver cysts are again seen on follow-up B-mode US (arrows in c) and confirmed on CEUS (arrows in d). No residual mass is seen inside the bladder on B-mode US (e) and on CEUS (f).

Fig 7. Two different patients with bladder removal. Patient 1: Urine collects in an external pouch. Double J catheters bilaterally are evident on radiograph (arrows in a). The distal ends terminate within the pouch. Proximal Cope loops are seen on US in the right (arrow in b) and left (arrow in c) renal collecting system. Patient 2: The bladder is replaced by an ileal conduit (d, e). The central renal collecting systems of the right (f) and the left (g) kidney show hydronephrosis.

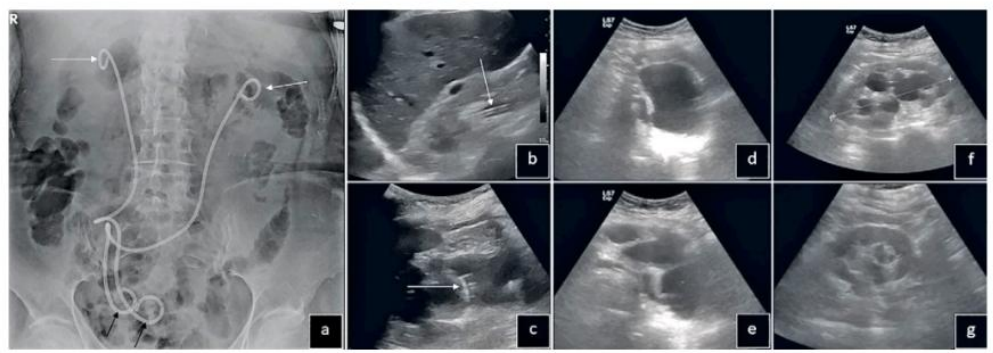

Intraneural ganglion cyst: an uncommon cause of foot drop

Po-Jia Pao, Yi-Hsiang Chiu, I-Chun Liu

Department of Physical Medicine and Rehabilitation, Cathay General Hospital, Taipei, Taiwan

To the Editor,

A 71-year-old man presented with two weeks of intermittent numbness in his left leg and weakness of the left ankle dorsiflexion. The numbness area ranged from the fibular head to the dorsum of the foot. He denied a history of prolonged left lateral decubitus position or recent trauma. His surgical history included pars repair due to L5/S1 spondylosis.

On physical examination, the muscle power of the left ankle dorsiflexion and eversion was 4, while ankle inversion was preserved. Steppage gait owing to the foot drop was noted when walking. Nerve conduction studies of the left peroneal nerve disclosed a conduction block between the above and below segments of the fibular neck. Additionally, a reduced amplitude of the sensory nerve action potential in the left superficial peroneal nerve was noted. These results implied left peroneal neuropathy across the fibular head. However, plain films demonstrated no spur or misalignment at the lateral component of the left femorotibial joint.

Further imaging studies were arranged to clarify etiology. Ultrasound revealed anechoic cystic lesions with posterior acoustic enhancement within the common peroneal nerve (fig 1A,B). No hypervascularity was noted around the lesion. Magnetic resonance imaging revealed multiple variably-sized, small cystic lesions at the anterolateral aspect of the fibula neck and mild edema in the anterior compartment muscle (fig 1C). No nerve root compression at the lumbosacral region was noted. Based on the findings, intraneural ganglion cysts at the left common peroneal nerve near the bifurcation were tentatively

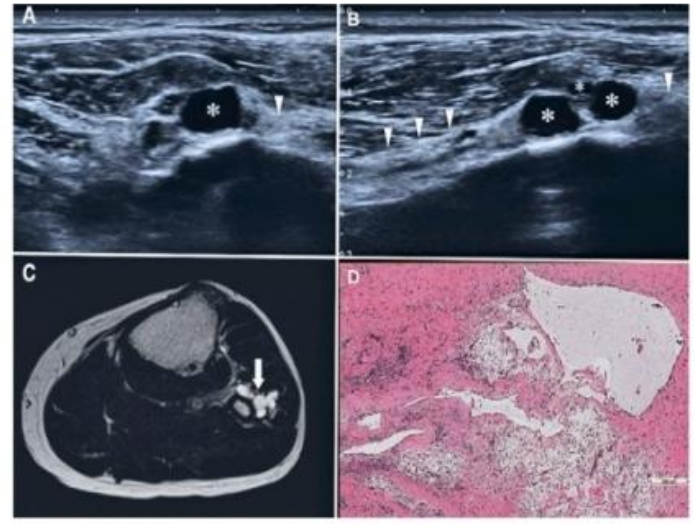

Fig 1. Ultrasound imaging at the level of the left fibular head in (A) a transverse view and (B) a longitudinal view revealed anechoic cystic lesions (asterisk) with posterior acoustic enhancement within the left common peroneal nerve (arrowhead). (C) Axial T2 weighted magnetic resonance imaging disclosed multiple variably sized, hyperintensity cystic lesions (arrow). (D) The specimen with a brown and elastic appearance, measuring 1.9x1.6x0.7 cm, was reported to be the ganglion cyst.

Received 08.02.2025 Accepted 23.02.2025
Med Ultrason
2025, Vol. 27, No 2, 241-242, DOI: 10.11152/mu-4512,
Corresponding author: I-Chun Liu, MD
Department of Physical Medicine and Rehabilitation, Cathay General Hospital
280 Renai Rd. Sec.4, 10630 Taipei, Taiwan
E-mail: jacy50521@gmail.com

Analysis of a case with unilateral submandibular gland agenesis accompanied by ipsilateral sublingual gland cyst and calculi

Xiurong Wang[1], Yanan Li[2,3], Xin Li[3], Qingna Xiao[3], Qiaozhen Liu[3], Miao Shi[3]

[1]Department of Ultrasound, Jinan Zhangqiu District People's Hospital, Jinan, [2]School of Medical Imaging, Ultrasound, Liaocheng People's Hospital, Liaocheng,

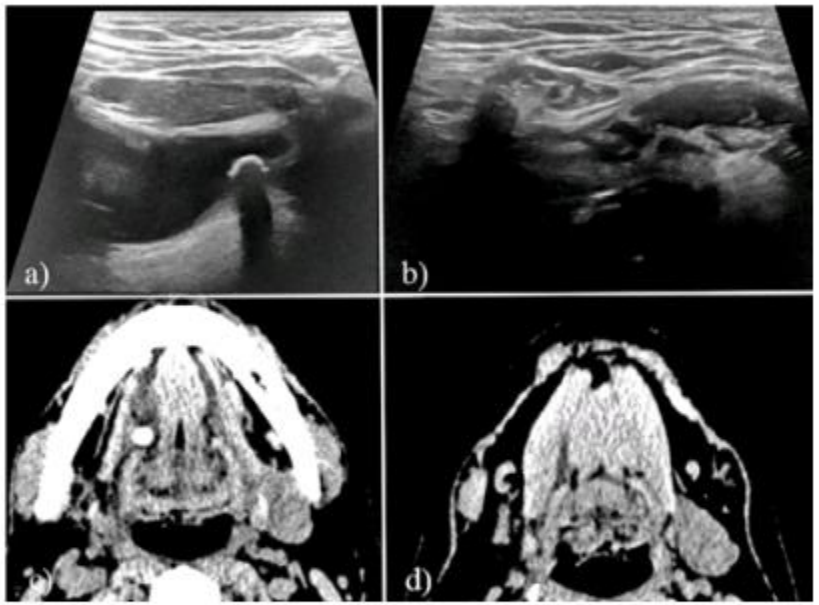

Fig 1. a) Anechoic area (3.5×2.6 cm) in right sublingual gland region containing hyperechoic focus (0.6×0.4 cm) with acoustic shadow; b) No gland tissue detected in right submandibular gland region; c) Nodular high-density image in right oral floor; d) Right submandibular gland poorly visualized.

To the Editor,

A 38-year-old male patient presented with a mass in the right sublingual area which appeared approximately 3 weeks before the presentation. Since its discovery, the patient had felt the mass gradually increasing in size. On physical examination, a mass approximately 1.5×1×1 cm was palpated in the right sublingual floor of the mouth. Ultrasound examination revealed a cystic mass in the right sublingual gland area with echogenic foci resem-

Inhomogeneity of the lacrimal glands is the most important ultrasound finding in primary Sjögren's syndrome: a comprehensive study with 2D-Shear Wave Elastography

Maria Badarinza, Oana Serban, Michael Andrei Pelea, Roxana Rosca, Lavinia Manuela Lenghel, Delia Doris Donci, Daniela Fodor

Abstract

Aim: This study aimed to compare the diagnostic performance, interobserver reliability, and practical utility of two lacrimal gland ultrasound (LGUS) scoring systems – LGUS score I, a complex multi-parameter score, and LGUS score II, a simplified single-parameter score – for diagnosing primary Sjögren's syndrome (pSS). The additional role of two-dimensional shear wave elastography (2D-SWE) in assessing lacrimal gland stiffness was also evaluated.

Material and methods: This observational, cross-sectional study included 35 pSS patients and 35 age- and sex-matched healthy controls. LGUS score I incorporated four grey-scale ultrasound parameters, while LGUS score II relied solely on glandular homogeneity. Both scoring systems were evaluated for diagnostic accuracy and interobserver agreement. SWE measurements of lacrimal gland elasticity were also recorded and compared between groups.

Results: LGUS score II achieved diagnostic performance comparable to LGUS score I, with areas under the curve (AUC) of 0.831 and 0.829, respectively (p=0.961). Sensitivity was higher for LGUS score II (94.29%) than for LGUS score I (85.70%), with both scores demonstrating identical specificity (68.57%). Interobserver agreement was good for LGUS score II (κ=0.707) and moderate for LGUS score I (κ=0.553). SWE measurements showed no significant differences in mean elasticity values between the pSS and control groups (8.78±2.03 kPa vs. 9.27±2.07 kPa, p=0.158).

Conclusion: LGUS score II (glandular homogeneity) offers a reliable, time-efficient diagnostic approach for pSS, providing similar accuracy to the more complex LGUS score I with enhanced interobserver reliability, while the potential of 2D-SWE remains limited by methodological inconsistencies and requires further standardization.

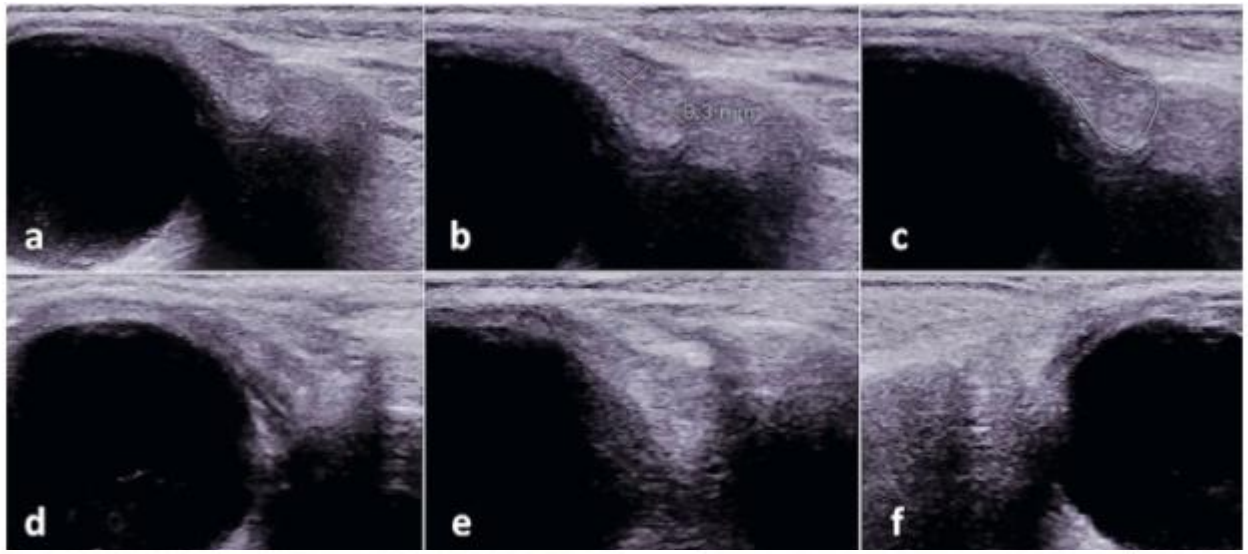

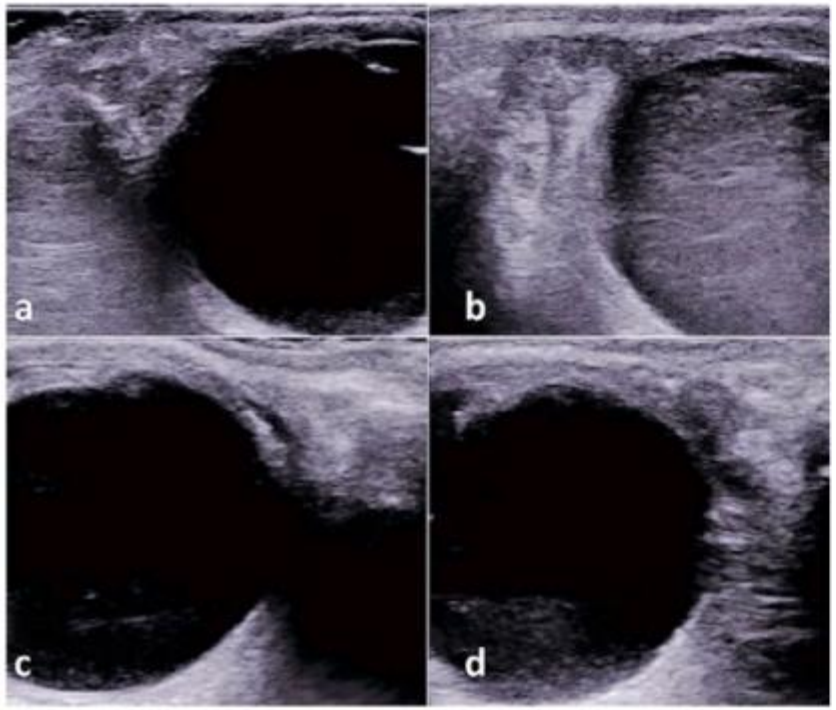

Fig 2. Lacrimal glands grey scale ultrasound parameters included in the score I: a) hypoechoic areas, b) hyperechoic bands, c) inhomogeneity of the parenchyma and d) irregular glandular contour

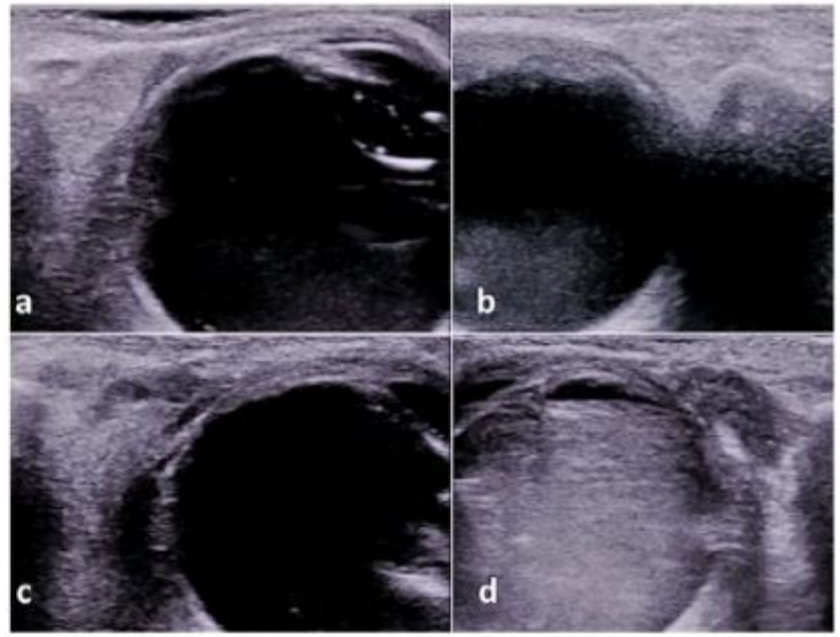

Fig 3. Grey scale grading included in LGUS score II: a) grade 0, homogeneous parenchyma, b) grade 1, mild heterogeneity without hypoechoic regions, c) grade 2, moderate heterogeneity with focal hypoechoic regions surrounded by normal parenchyma, d) grade 3, diffuse heterogeneity with hypoechoic regions without normal parenchyma

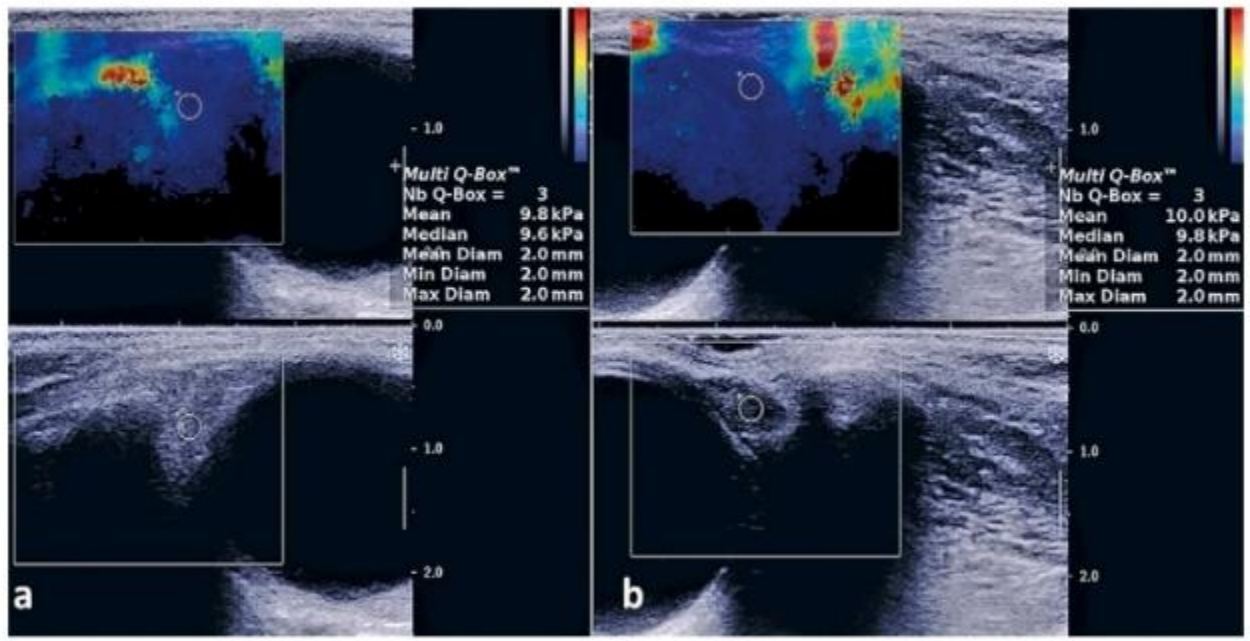

Fig 4. Two-dimensional shear wave elastography (2D-SWE) of the lacrimal glands in a) healthy individuals and b) primary Sjögren Syndrome patients

← Back to Ultrasound Journal

3 February, 2025

Ultrasound evaluation of gallbladder wall thickness for predicting severe dengue: a systematic review and meta-analysis

Amirhossein Shahsavand Davoudi, Hamid Harandi, Reza Samiee, Shayan Forghani, Keyhan Mohammadi and Maryam Shafaati

Review | Open access | Published: 03 February 2025

Ultrasound evaluation of gallbladder wall thickness for predicting severe dengue: a systematic review and meta-analysis

Amirhossein Shahsavand Davoudi, Hamid Harandi, ...

Maryam Shafaati ✉ + Show authors

The Ultrasound Journal **17**, Article number: 12 (2025)

The Ultrasound Journal

REVIEW Open Access

Ultrasound evaluation of gallbladder wall thickness for predicting severe dengue: a systematic review and meta-analysis

Amirhossein Shahsavand Davoudi[1], Hamid Harandi[1,2], Reza Samiee[1], Shayan Forghani[1], Keyhan Mohammadi[2,3] and Maryam Shafaati[2*]

Abstract

Background The prevalence of dengue fever (DF), a mosquito-borne viral disease, is rising worldwide. Its severe manifestations like thrombocytopenia and plasma leakage are associated with increased mortality. Ultrasound-detected gallbladder wall thickening (GBWT) has been suggested as a potential indicator of the severity of the disease.

Aims This systematic review and meta-analysis evaluated the predictive value of GBWT in identifying patients at risk for severe dengue.

Methods Following the PRISMA 2020 guidelines, we conducted a systematic search of Web of Science, PubMed, Embase, and Scopus. Among the inclusion criteria were original studies that assessed GBWT across various dengue severity categories. Then, we performed a meta-analysis using a random effects model and subgroup analyses based on severity criteria to determine the relationship between GBWT and severe dengue.

Results For the meta-analysis, 19 studies qualified for the inclusion criteria. There was a significant association between GBWT and severe dengue, according to the odds ratio (OR) of 2.35 (95% CI 1.88–2.82, $p < 0.001$). The subgroup analysis revealed consistent results for thrombocytopenia (OR: 2.65) and plasma leakage (OR: 2.26), among other severity criteria.

Conclusions A reliable ultrasound indicator, GBWT can help identify patients at risk for severe dengue early on, improving clinical decision-making and patient outcomes. However, the possibility of differential diagnosis requires cautious interpretation.

Keywords Dengue fever, Severe dengue, Gallbladder wall thickening (GBWT), Ultrasound, Risk prediction

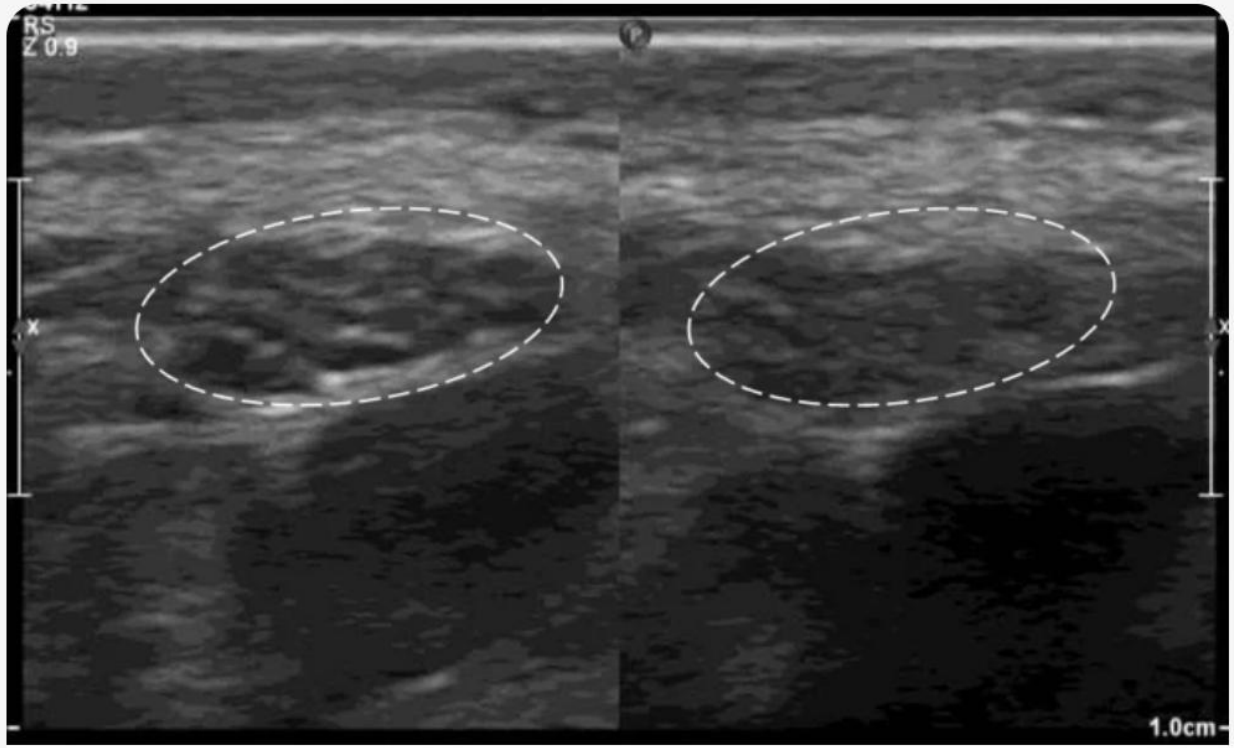

Peripheral nerve ultrasound: a survival guide for the practicing radiologist with updates

28 March, 2025

26 March, 2025

Peripheral nerve ultrasound: a survival guide for the practicing radiologist with updates

Mohamed Ragab Nouh, Hoda Mohamed Abdel-Naby, Tarek El Sakka & Mohamed El-Shafei

Abstract

Peripheral nerve injuries significantly impact patients' quality of life and place a burden on healthcare resources. This review explores the application of high-resolution neurosonography (HRNUS) in mapping peripheral nerves and identifying pathological lesions.

It underscores HRNUS's role in diagnosing nerve disorders and outlines widely accepted classification schemes for peripheral nerve injuries.

The article highlights HRNUS's non-invasive, flexible, patient-friendly, and cost-effective attributes, advocating for its use to achieve accurate diagnoses, prevent permanent disabilities, and optimize healthcare resource utilization.

Fig. 1

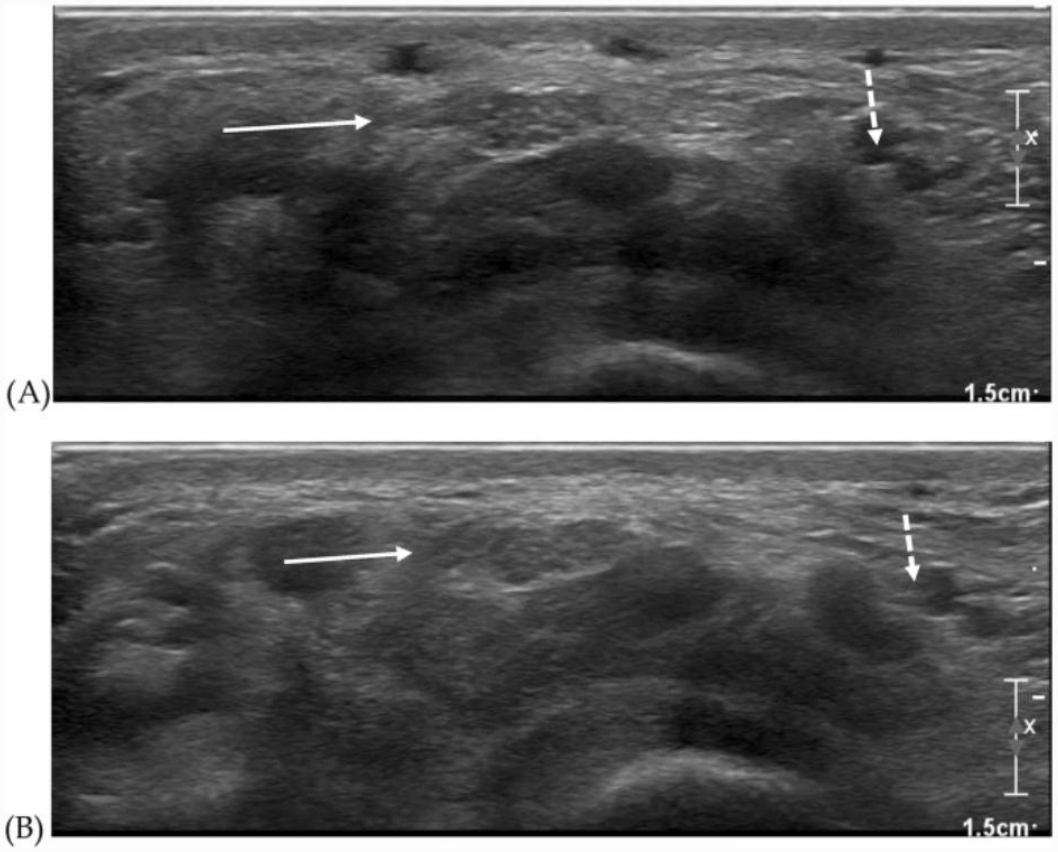

Highlights the crucial role of proper focus adjustment in achieving clear internal neural texture. Axial images **A** and **B** depict the honeycomb pattern of the median (solid arrow) and ulnar (dashed arrow) nerves at different focus levels. **A** Shows the nerves in focus, while **B** has a deeper focus, leading to a loss of the honeycomb appearance due to improper adjustment. The effect is more noticeable in the ulnar nerve due to anisotropy

Fig. 2

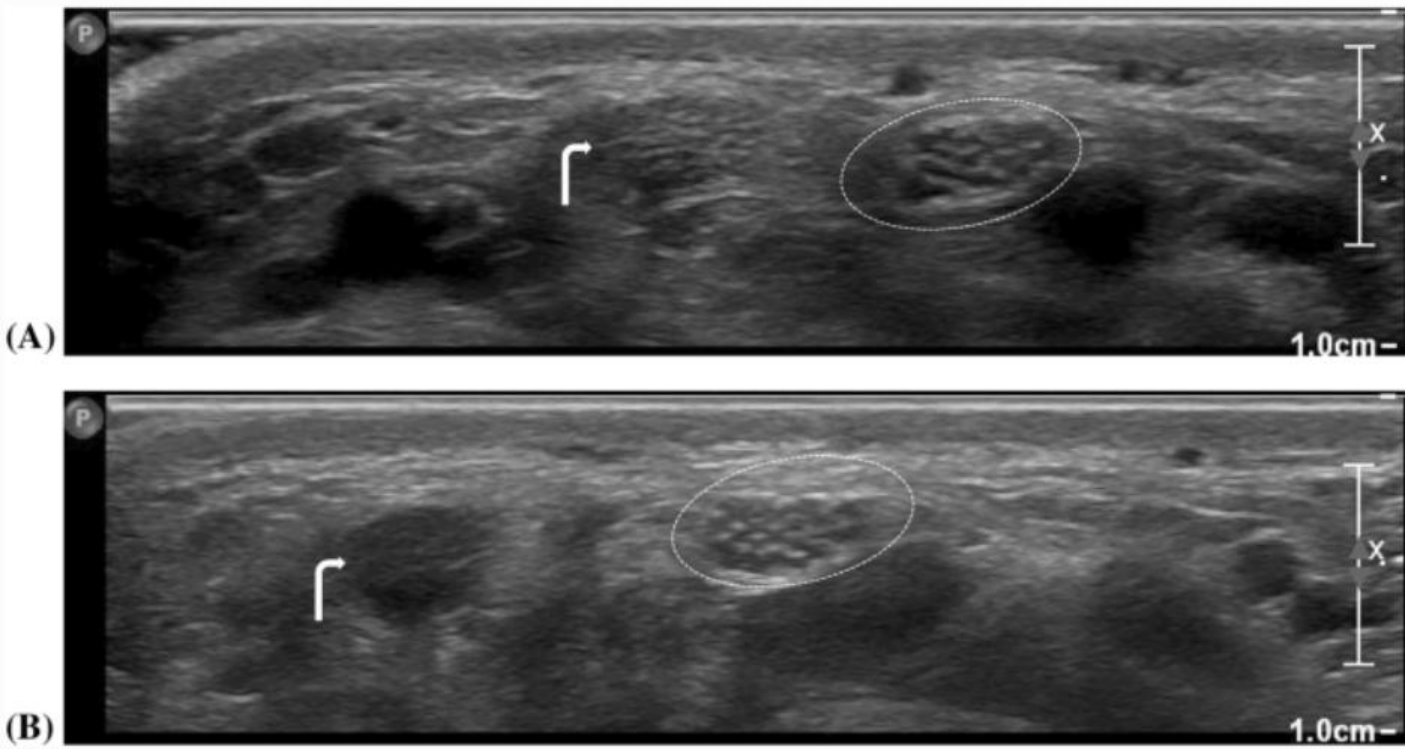

Illustrates the phenomenon of anisotropy, which affects tendons more than nerves. Two images **A** and **B**, of a normal individual's left-side wrist, showing the median nerve (dashed ellipse) and the adjacent flexor carpi radialis tendon (bent arrows). The images have identical parameters except for probe angulation. The median nerve's normal fascicular axial appearance is clear in **A** but slightly muffled in **B**. The flexor carpi radialis tendon's axial appearance is visible in **A** but shadowed in **B** while other tendons appear muffled in both images. M and L refer to medial and lateral directions

Fig. 4

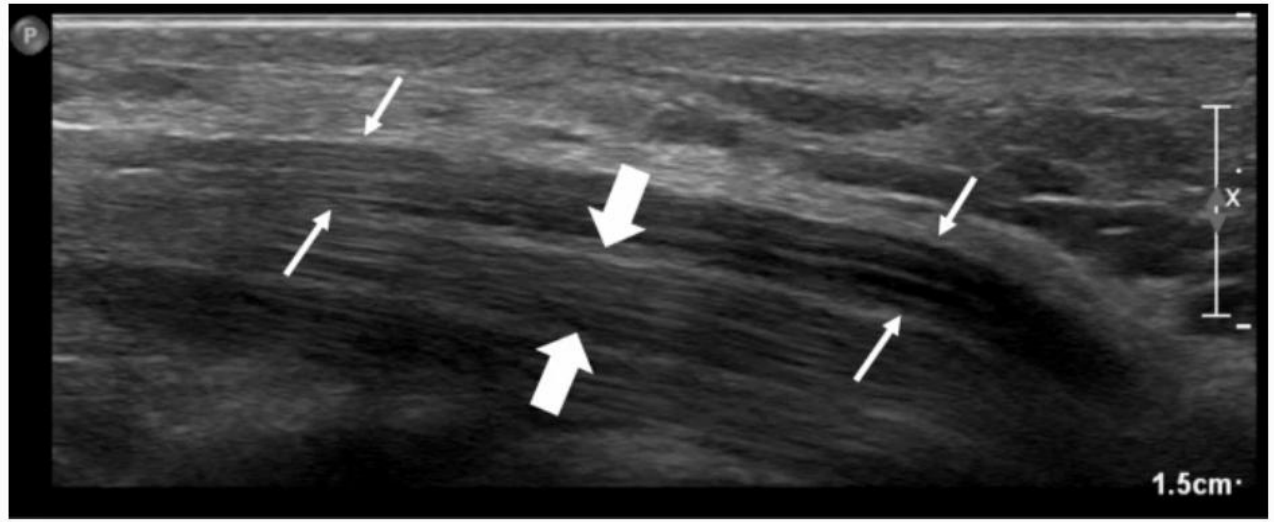

Shows the median nerve (marked between small arrows) and a parallel tendon (marked between block arrows) in the forearm, with the nerve having a tram-track appearance and the tendon having a more compact internal structure. Anisotropy may cause similarity, making differentiation difficult, especially on the left side of the image

Fig. 5

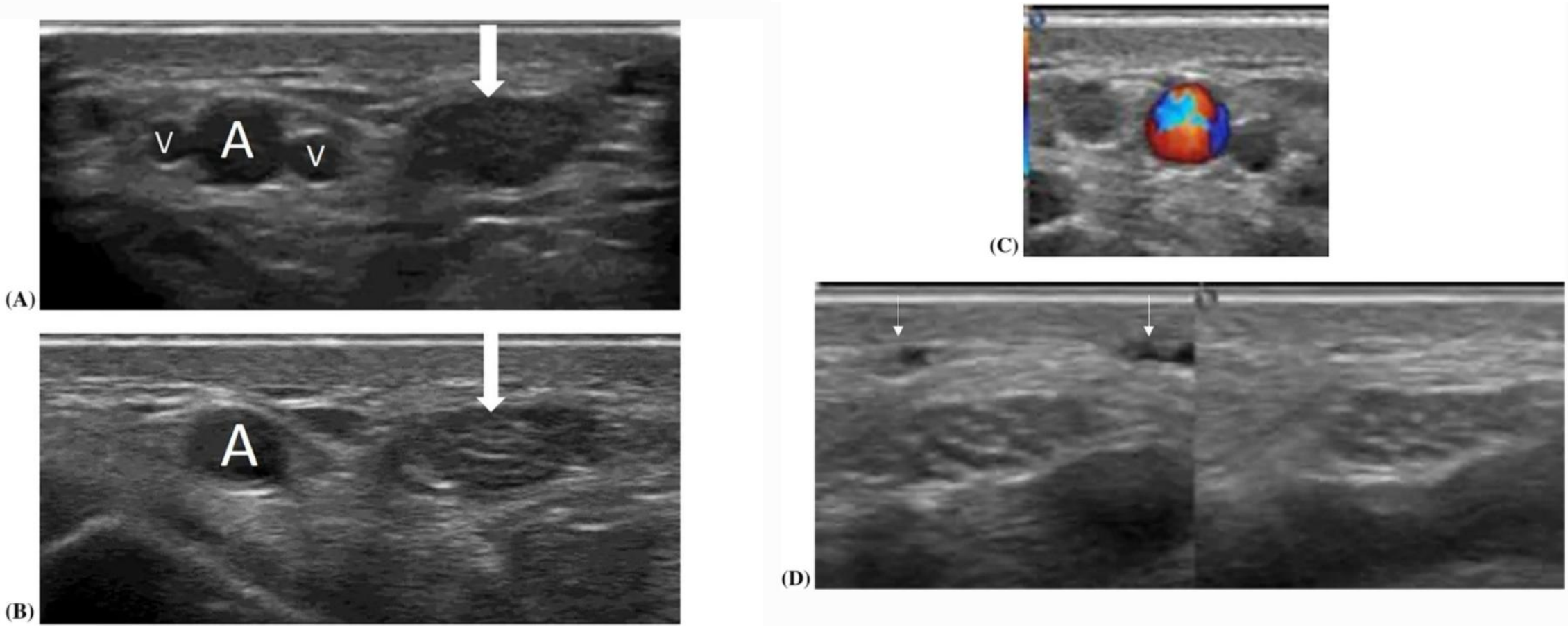

Original article | Open access |
Published: 13 January 2025

Validation of a tele-robotic ultrasound system for abdomen and thyroid gland explorations: a comparison with standard ultrasound

Andreu Antolin ✉, Nuria Roson, … Manuel Escobar

Thyroid gland protocol

The protocol used for the assessment of thyroid gland requires the patient to be in supine position with neck hyperextension. The transducer is placed in axial orientation in the infrahyoid neck, in the midline, for a full view of the thyroid gland and the isthmus. The transducer is then displaced to right and left to assess both thyroid lobes in short and long axis. Afterwards, the main cervical vessels from both sides are assessed moving the transducer a little bit more laterally. Finally, the right and left submandibular glands are evaluated in the submandibular space with the patient doing a head tilt to the left and right respectively.

An assistant was present in each tele-robotic US examination to assist in the procedure. The role of the assistant is to welcome the patient and ensure that the study is performed without any inconvenience. The assistant accommodates the patient and has direct communication with the radiologist to apply sonographic gel, relocate the robotic arm or camera, assist with the patient's movements or solve any other potential issues. Patient-site assistants had no prior training in US but were instructed in basic operations of using the system, including turning on and off each component of the system and using the emergency button for shutting down the robotic arm.

The standard US protocol was similar to the previously described with variations depending on the radiologists and the specific clinical request in outpatients.

Tele-robotic US protocol

Abdominal protocol

The abdominal protocol requires the patient in supine position with the arms behind the head. The examination begins with the transducer placed in sagittal orientation in the epigastric region to assess the left hepatic lobe in different planes. Afterwards it follows the anterior subcostal plane to continue the examination of the rest of the liver and related structures. Then the patient is asked to tilt a little bit towards the left to access the intercostal spaces, and then is positioned in almost complete left lateral decubitus to be able to examine the right kidney. Posteriorly, the patient is asked to move to a supine position to examine the pancreatic region in the epigastrium. To continue with the left hypochondrium structures and left kidney the patient is asked again to move to an incomplete or complete right lateral decubitus to assess the spleen and left kidney. Finally, the patient returns to the standard supine position to evaluate the retroperitoneal main vessels and afterwards the urine bladder in axial and sagittal plane in the hypogastric region. The patient's position is slightly modified in the different steps described based on the morphological characteristics and is asked to help with breathing to better depict the evaluated structures.

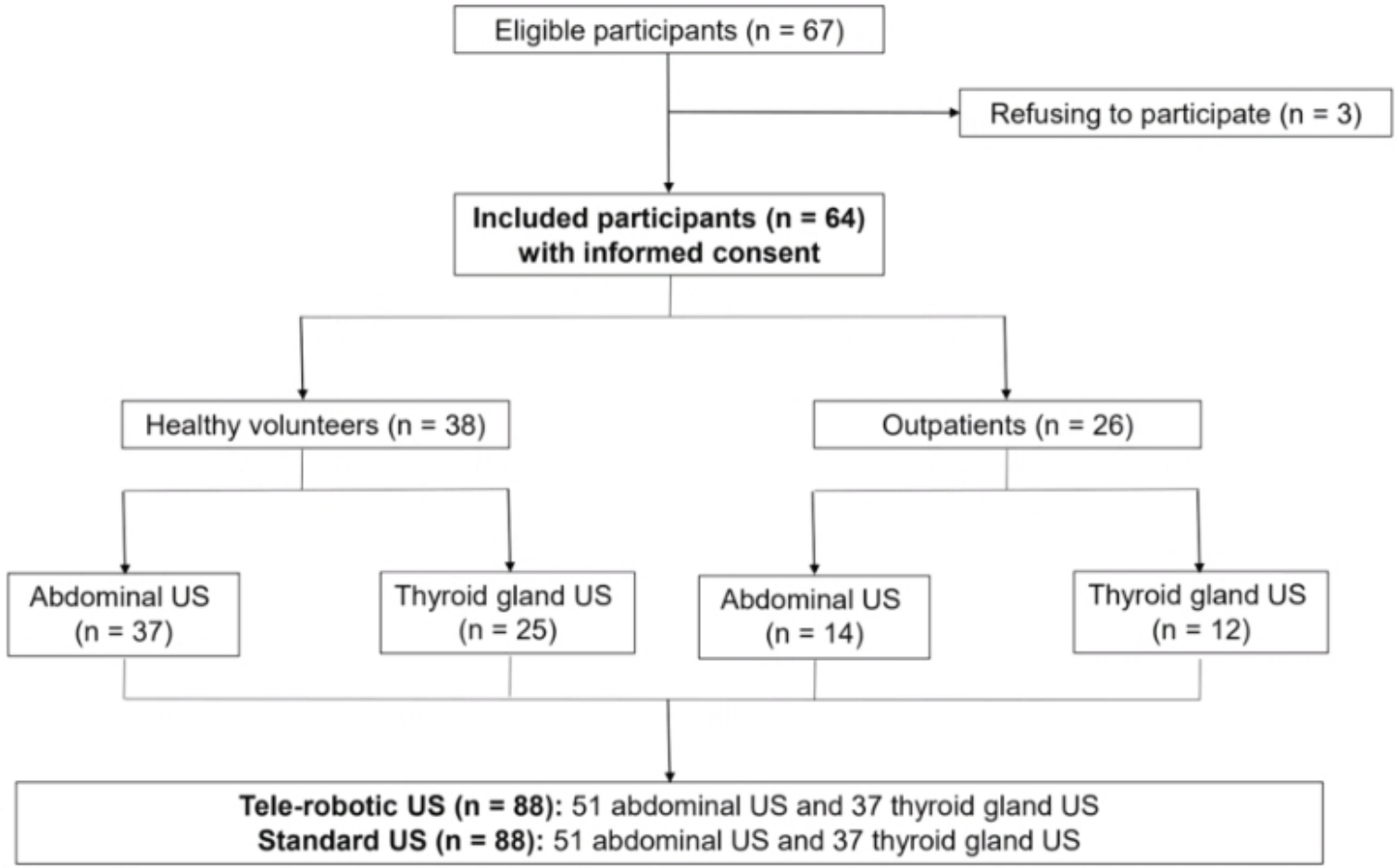

Fig. 1 Flow diagram of the participants included in the study divided in healthy volunteers and outpatients, with the total amount of abdominal and thyroid ultrasounds (US)

Table 1 Participants' basic demographics and characteristics

Table 2 List of the specific clinical requests for abdominal and thyroid gland ultrasounds of the outpatients

Requests for Abdominal Ultrasound
2 patients with cholestasis and right mild hypochondrial pain
1 patient with transaminitis and psoriatic arthritis previously treated with methotrexate
5 patients with transaminitis and no specific clinical symptom
1 patient with clinical suspicion of Gilbert syndrome
1 patient with microhematuria
1 patient that referred history of renal lithiasis
1 patient with long-standing liver transplant, referred for periodic follow-up
1 patient with 2 focal nodular hyperplasia for annual follow-up
1 patient referred to characterize hypodense lesions in left hepatic lobe seen in CT
Requests for Thyroid Gland Ultrasound
1 patient with adenomatous familial polyposis syndrome referred to rule out papillary thyroid carcinoma
7 patients with nodular thyroid disease, including 4 multinodular goiters
2 patients with recent diagnosis of hypothyroidism
1 patient with clinical background of breast cancer and a hypermetabolic right thyroid nodule seen in PET-CT
1 patient with normocalcemic hyperparathyroidism

Ahead of print

Med Ultrason 2024:0, 1-11 Online first
DOI: 10.11152/mu-4451

Ultrasound measurements and normal findings in the thyroid gland

Saubhagya Srivastava[1], Manjiri Dighe[1], Kathleen Möller[2], Maria Cristina Chammas[3], Yi Dong[4], Xin-Wu Cui[5], Christoph Frank Dietrich[6]

[1]University of Washington, Washington, Seattle, Washington, USA, [2]Medical Department I/Gastroenterology; SANA Hospital Lichtenberg, Berlin, Germany, [3]Hospital das Clínicas da Faculdade de Medicina da Universidade de São Paulo, Instituto de Radiologia, São Paulo, Brazil, [4]Department of Ultrasound, Xinhua Hospital, Shanghai Jiao Tong University School of Medicine, Shanghai, China, [5]Department of Medical Ultrasound, Tongji Hospital, Tongji Medical College, Huazhong University of Science and Technology, Wuhan, China, [6]Department General Internal Medicine (DAIM), Hospitals Hirslanden Bern Beau Site, Salem and Permanence, Bern, Switzerland

Abstract

The present work describes the process of the sonographic examination, normal findings and measurements in the B-mode ultrasound evaluation. Reference is made to anatomical variants in shape, the pyramidal lobe, tubercle of Zuckerkandl, ectopic thyroid tissue, and their significance. Particular attention is paid to the reference values, the very miscellaneous reference values in different geographic regions of the world and influencing factors.

Keywords: Thyroid gland; Ultrasonography; reference values; anatomical variants

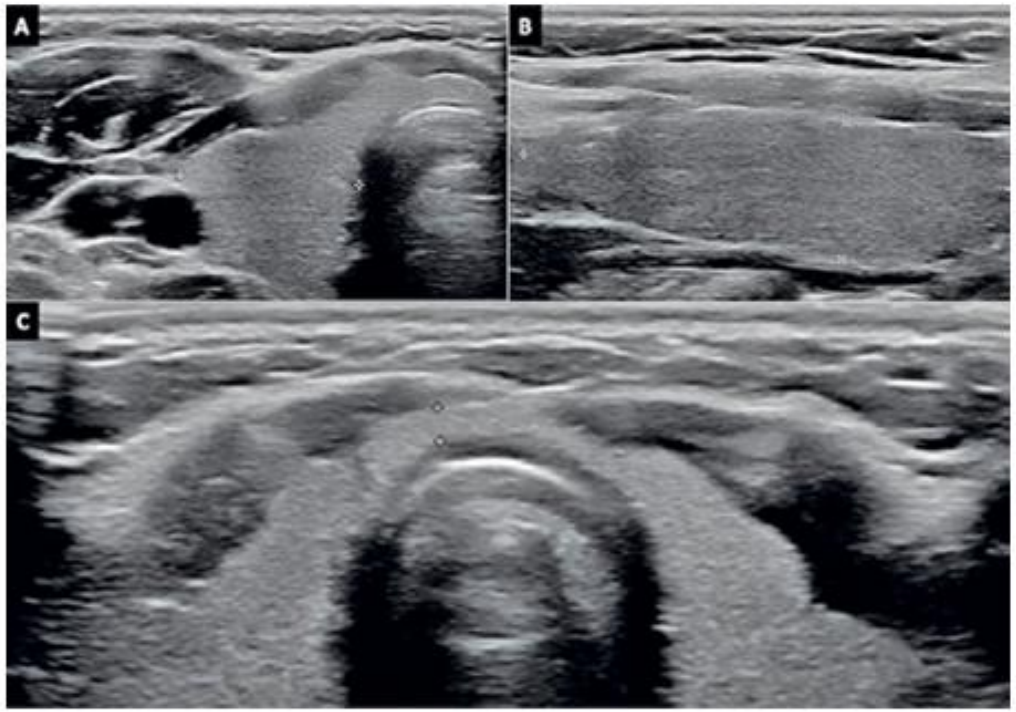

Fig 6. Thyroid measurements. Transverse dimensions of the right thyroid lobe (+ calipers) (A). Sagittal image showing the anteroposterior (AP) measurement (x calipers) and longitudinal measurements (+ calipers). (C) Transverse image showing the AP measurement of the thyroid isthmus (+ calipers) (B).

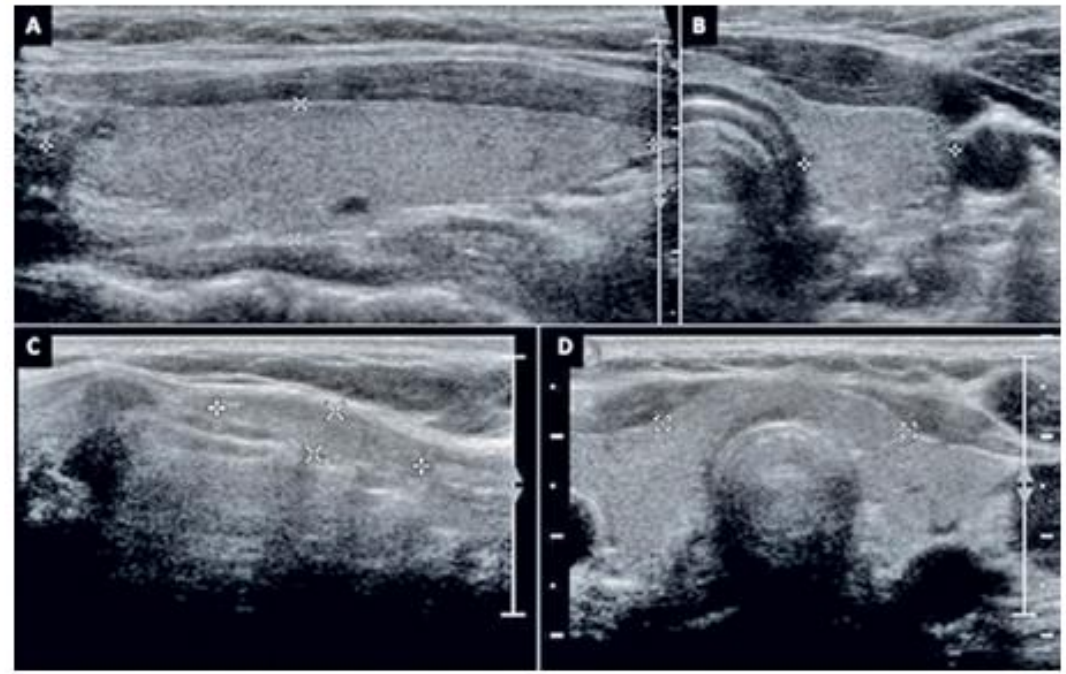

Fig 7. Thyroid measurements. Longitudinal (A) and transverse (B) sections dimensions of the left thyroid lobe (+ calipers). Longitudinal (C) and transverse (D) sections of the isthmus, show the measurements.

Table I. Thyroid reference values in neonates, at 1 year and in adults and velocities in superior and inferior thyroid arteries.

Characteristic		Normal reference values
Size	Neonate	Sagittal: 1.8-2.0 cm AP: 0.8-0.9 cm
	At 1 year	Sagittal: 2.5 cm AP: 1.2-1.5 cm
	Adult	Sagittal: 5.0 cm AP: 2.0 cm Transverse: 2.0 cm (5x2x2 cm)
Volume	Neonate	0.40 – 0.14 mL
	Children	Increases at a rate of 1.0-1.3 mL for every 10 kg body weight gained
	Adult	10-11±3 mL
Mean peak systolic velocities	Superior thyroid artery	25.9 cm/s
	Inferior thyroid artery	21.5 cm/s

Table II. Studies that evaluated the reference values in ultrasound examination of the thyroid, which can be used for Caucasians.

Study	Size	Volume	Congenital and shape abnormalities
Richman et al [6]	Adult: 5 cm x 2 cm x 2 cm (sagittal x anteroposterior x transverse)	-	Partial or complete congenital absence of the thyroid Pyramidal lobe Zuckerkandl tubercle Thyroglossal duct remnant
Viduetsky et al [17]	-	10 - 15 mL for females; 12 - 18 mL for males	-
Peterson et al [36]	-	10.5 mL	The shape error was due to the fact that individual thyroid lobes differ substantially from the perfect rotation-ellipsoid

Table V. Causes of changes in the size of the thyroid gland.

Causes of changes in the size of the thyroid gland	
Too big	**Too small**
Iodine deficiency, Struma diffusa	After radioiodine therapy
Struma nodosa, thyroid nodules	Final state of Hashimoto thyroiditis
Thyroiditis • Graves' /Basedow´s disease • Hashimoto Thyroiditis • Thyroiditis de Quervain • Postpartum Thyroiditis	Autoimmune/ Ord's hypothyroidism Radiotherapy for head and neck cancer
High body surface area	
Decreased TSH-level, hyperthyroidism	
Medication (Lithium, Acetylsalicylic acid, excessive large doses of iodine)	
Goitrogenic foods: onions, manioc, soy, tofu, walnuts and peanuts or in many types of cabbage	
Pregnancy	